nanomaterials

MDPI

Article

Composites of Montmorillonite and Titania Nanoparticles Prepared by Inverse Microemulsion Method: Physico-Chemical Characterization

Alicja Michalik, Bogna D. Napruszewska, Dorota Duraczyńska, Anna Walczyk and Ewa M. Serwicka *

Jerzy Haber Institute of Catalysis and Surface Chemistry, Polish Academy of Sciences, Niezapominajek 8, 30-239 Krakow, Poland

* Correspondence: ncserwic@cyf-kr.edu.pl; Tel.: +48-12-6395-118

Abstract: TiO_2/montmorillonite composites were synthesized using inverse micellar route for the preparation of titania nanoparticles (4–6 nm diameter) in 1-hexanol and for the dispersion of one of the clay components. Two series of composites were obtained: one derived from cetyltrimethylammonium organomontmorillonite (CTA-Mt), exfoliated in 1-hexanol, and the other from sodium form of montmorillonite (Na-Mt) dispersed by formation of an inverse microemulsion in 1-hexanol. The TiO_2 content ranged from 16 to 64 wt.%. The composites were characterized with X-ray diffraction, scanning/transmission electron microscopy/energy dispersive X-ray spectroscopy, thermal analysis, and N_2 adsorption-desorption isotherms. The Na-Mt-derived component was shown to undergo transformation to CTA-Mt, as indicated by basal spacing of 17.5 nm, due to the interaction with the CTABr surfactant in inverse microemulsion. It was also better dispersed and intermixed with TiO_2 nanoparticles. As a result, the TiO_2/Na-Mt series displayed superior textural properties, with specific surface area up to 256 m^2g^{-1} and pore volume up to 0.247 cm^3g^{-1} compared with 208 m^2g^{-1} and 0.231 cm^3g^{-1}, respectively, for the TiO_2/CTA-Mt counterpart. Members of both series were uniformly mesoporous, with the dominant pore size around 5 nm, i.e., comparable with the dimensions of titania nanoparticles. The advantage of the adopted synthesis method is discussed in the context of other preparative procedures used for manufacturing of titania-clay composites.

Keywords: TiO_2; clay; montmorillonite; organoclay; composite; inverse microemulsion; inverse micelle; mesoporosity

Citation: Michalik, A.; Napruszewska, B.D.; Duraczyńska, D.; Walczyk, A.; Serwicka, E.M. Composites of Montmorillonite and Titania Nanoparticles Prepared by Inverse Microemulsion Method: Physico-Chemical Characterization. *Nanomaterials* **2023**, *13*, 686. https://doi.org/10.3390/nano13040686

Academic Editor: Vasco Teixeira

Received: 31 December 2022
Revised: 30 January 2023
Accepted: 6 February 2023
Published: 10 February 2023

1. Introduction

Titania-based composites are widely researched materials whose potential in heterogeneous catalysis and especially photocatalysis has long been recognized [1]. In catalysis, the TiO_2 component is generally used as a catalyst carrier because it displays an advantageous combination of chemical inertness, resistance to poisoning, and the ability to interact with the supported active phase. In photocatalysis, titania plays the role of the actual catalyst, which, when subjected to bandgap illumination, enables generation of holes and electrons participating in the photochemical reaction.

The use of titania in the form of nanoparticles is particularly attractive because it ensures a high surface-to-volume ratio and high density of coordinatively unsaturated sites. This in turn affects the oxide stoichiometry, structure, electronic characteristics, and related properties such as, e.g., acido-basicity [2]. However, the use of nanoscale particles is burdened with the general challenges associated with their handling. The potential problems include the trickiness of nanoparticles separation and recovery from the reaction medium, the tendency to cluster at higher concentrations, or proneness to sintering at high temperatures [3,4]. These difficulties can be defused by anchoring the nanoparticles onto supports, the approach widely used in the design of titania-based systems. A great number of different inorganic and organic matrices have been used in the capacity of supports

for TiO_2 species. The examples include silica, zeolites, glass, clay minerals, carbonaceous materials, or organic polymers [5]. The naturally occurring clay minerals are of particular interest because they display an exceptional combination of advantageous properties, i.e., non-toxicity, abundance, low cost, and unique layered structures. The lamellar lattice elements may be considered as prefabricated building blocks ready to be used in advanced materials syntheses [6]. In addition, clay mineral surfaces are capable of physi- and/or chemisorption, which may be beneficial for enhancement of reagents concentration around the supported nanoparticles [7]. Several recent reviews reflect the widespread interest in various aspects of titania-clay composites synthesis and applications [1,8–12].

Montmorillonite is the mineral most frequently used in the capacity of clay component. Its cation exchange capacity and swellability are key properties controlling formation of the composites, and a variety of preparative approaches have been adopted in the past to design hybrids with TiO_2 [1]. The most often employed procedure is referred to as pillaring. It results in the localization of polymeric Ti species in the interlayer, thereby increasing the layer spacing while maintaining the stacking order of the layers. Another type of nanoarchitecture is formed when TiO_2 nanoparticles become trapped between disordered, exfoliated montmorillonite layers. This type of structure is called a house of cards assembly. Alternatively, when the synthesis conditions prevent cation exchange and/or swelling, the titania nanoparticles become attached to the external surfaces of the mineral grains. This type of TiO_2 deposition is usually the case during montmorillonite impregnation with the Ti precursor but may also appear in addition to the interlayer loading.

The common method used for generation of titania species to be embedded in the composite structure is the in situ or ex situ hydrolysis of inorganic or organic precursor [1]. Recently, we described a novel strategy for design of metal oxide/clay composites based on the use of exfoliated layered organoclays but with oxide nanoparticles obtained from oxo-hydroxy precursors prepared in water-in-oil (w/o) inverse microemulsions [13–15]. Inverse microemulsions, also referred to as reverse microemulsions, are thermodynamically stable and optically transparent dispersions of aqueous microdroplets in a continuous oil phase and stabilized by the presence of surfactant molecules at the water–oil interface [16]. In the ternary water-oil-surfactant phase diagram, the region in which the inverse micelles are formed is usually found near the oil apex of the triangle [17]. Mixing of inverse microemulsions containing appropriate reactants in aqueous micellar cores results in coalescence of micelles and precipitation of nanoparticles, with size limited by the dimensions of micellar interior. Moreover, the variation of the water-to-oil ratio and surfactant concentration could influence the size of prepared nanoparticles. For this reason, the inverse microemulsion method has been widely used for the synthesis of variety of nanomaterials [16–19].

In the present work, we describe the application of the inverse micellar route to produce titania nanoparticles for the preparation of TiO_2/clay composites. The clay component, montmorillonite (Mt), was prepared in two different ways. In the first case, Mt was used as a cetyltrimethylammonium organoclay (CTA-Mt) to facilitate its exfoliation in the organic reaction medium (1-hexanol). In the other procedure, Na-montmorillonite (Na-Mt) was used. This form of clay mineral is hydrophilic and does not disperse in n-hexanol. To bypass this obstacle, we used a completely novel approach in which the Na-Mt component was prepared as an inverse microemulsion in 1-hexanol, with clay mineral present as a suspension in aqueous micellar cores.

2. Materials and Methods

2.1. Materials

The starting montmorillonite (Mt) used for the preparation of composites was the sodium form of the less than 2 μm particle size fraction separated by sedimentation from Jelšový Potok (JP) bentonite (Slovakia) provided by ZGM Zebiec (Starachowice, Poland). The JP deposit contains montmorillonite as the only clay mineral phase [20].

The ternary system water/cetyltrimethylammonium bromide (CTA-Br)/1-hexanol with well-known phase diagram [21] was chosen for the preparation of microemulsions.

Based on this diagram, the weight proportion of aqueous phase:CTABr:1-hexanol equal 17:28:55 was selected for the preparation of inverse microemulsions. The mixture is characterized by the molar water-to-surfactant ratio w_0 = 11.75. Parameter α (the ratio of oil phase mass to the sum of oil and aqueous phase masses) is =0.76, and parameter γ (the ratio of surfactant mass to the sum of oil, water, and surfactant masses) is 0.28.

The following reactants, denoted as A, B, C, and D, were used in the composite syntheses:

A. The sodium form of montmorillonite, denoted as Na-Mt, was obtained by cation exchange of parent clay with excess of 1 M NaCl solution, washed by centrifugation with distilled water till negative reaction of the solute with $AgNO_3$, and stored in the form of a gelatinous paste (ca. 5 wt.% of clay);

B. The organomontmorillonite was prepared from Na-Mt by cation exchange with excess of cetyltrimethylammonium bromide (CTABr) aqueous solution, followed by washing with distilled water till negative reaction of the solute with $AgNO_3$. To remove excess water, the organic derivative, denoted as CTA-Mt, was washed three times with isopropanol, then three times with 1-hexanol, and stored in the form of a gelatinous paste (ca. 10 wt.% of clay);

C. The inverse Ti-containing microemulsion was prepared by adapting the approach proposed for the microemulsion synthesis of hydrous zirconia nanoparticles [22]. First, the Ti-containing aqueous phase was obtained by controlled hydrolysis of $TiCl_4$ [23]. In a typical experiment, 6.5 mL of 6 M HCl was added to 9 mL of $TiCl_4$ and diluted with 100 mL of distilled water. After stirring for 3 h at room temperature, a clear solution containing 3.7 wt.% of Ti was obtained. The Ti aqueous phase was mixed with CTABr and 1-hexanol in weight proportion 17:28:55 and stirred till the mixture turned into a dense transparent liquid, indicating formation of inverse microemulsion;

D. The microemulsion of NH_3aq, used for speeding up hydrolysis of the Ti precursor species, was obtained by mixing 25% NH_3aq, CTABr, and 1-hexanol in the selected weight proportion till the formation of clear solution.

$TiCl_4$ (ReagentPlus®), CTABr (≥98%), and 1-hexanol (for synthesis) were purchased from Sigma-Aldrich (Poznan, Poland); all other chemicals used in syntheses were of p.a. purity provided by Chempur (Piekary Slaskie, Poland).

Two methods of composite synthesis, differing by the manner of preparation of the clay mineral component, were used. Organomontmorillonite to be used in composite synthesis was prepared by dispersing reactant B in 1-hexanol to yield 0.5 wt.% suspension of CTA-Mt. Sodium montmorillonite was prepared as a microemulsion of Na-Mt by mixing reactant A with CTABr and 1-hexanol in weight proportion 17:28:55 and stirring the mixture till a clear, gray liquid containing ca. 0.9 wt.% Na-mt was obtained. Further synthesis stages were common for both the CTA-Mt and the Na-Mt components. The clay mineral dispersions were mixed with reactant C added in the amount providing the intended TiO_2 loading of 0.25, 0.5, 1, or 1.5 g per gram of montmorillonite component and heated to 60 °C. To accelerate Ti precursor hydrolysis, reactant D was added under stirring till the originally greyish suspensions turned white. The mixtures were kept under stirring at 60 °C for 30 min. After cooling down, the suspensions were washed by centrifugation with ethanol (3×), followed by washing with 1:1 water-ethanol mixture until free of bromide ions. Lyophilization of the precipitates yielded fine powders that were subjected to calcination for 4 h at 550 °C. The samples obtained from CTA-Mt are referred to as $0.25TiO_2$/CTA-Mt, $0.5TiO_2$/CTA-Mt, $1TiO_2$/CTA-Mt, and $1.5TiO_2$/CTA-Mt, while those prepared from Na-Mt are denoted as $0.25TiO_2$/Na-Mt, $0.5TiO_2$/Na-Mt, $1TiO_2$/Na-Mt, and $1.5TiO_2$/Na-Mt. A scheme of composite synthesis is shown in Figure 1.

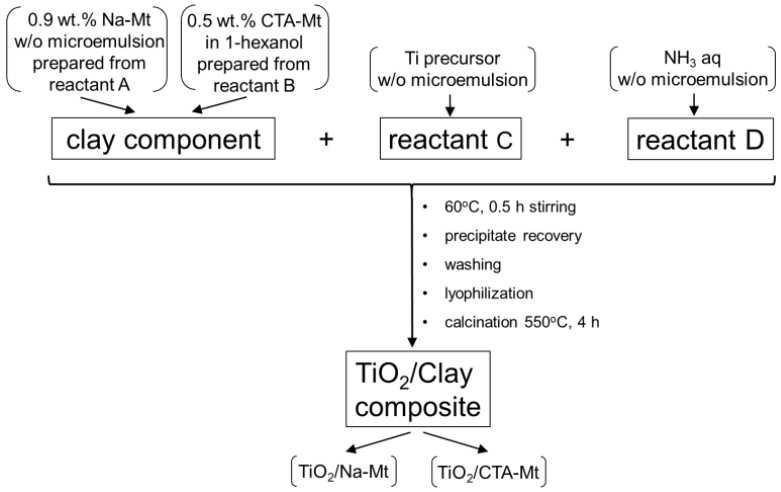

Figure 1. Schematic illustration of composite synthesis.

2.2. Methods

Powder X-ray diffraction (XRD) patterns were recorded using X'Pert PRO MPD diffractometer (PANalytical, Almelo, The Netherlands) with CuKα radiation. The crystallite sizes of TiO_2 nanoparticles (the size of coherently scattering domains) were estimated for the (101) reflection of anatase using the Scherrer formula and taking into account the instrumental broadening. Scanning/transmission electron microscopy/energy dispersive X-ray spectroscopy (SEM/TEM/EDX) study of the materials was carried out with aid of JEOL JSM-7500F Field Emission Scanning Electron Microscope (JEOL, Tokyo, Japan) coupled with an INCA PentaFetx3 EDX (Oxford Instruments, Abingdon, UK) system. SEM/TEM images were recorded for the uncoated samples deposited as suspensions on 200 mesh copper grids covered with carbon support film. An average of EDX measurements for 10 areas of ca. 1 μm × 1 μm, chosen at random on the sample surface, was used for determination of sample composition. N_2 adsorption/desorption at −196 °C was measured with an AUTOSORB 1 (Quantachrome, Boynton Beach, FL, USA) instrument. The samples were outgassed at 200 °C for 2 h. Brunauer–Emmett–Teller (BET) formalism was used for the calculation of specific surface areas (S_{BET}). The total pore volume (V_{tot}) was determined from the amount of N_2 adsorbed at $p/p_0 = 0.996$. Mesopore volume (V_{meso}) was determined from the adsorption branch using the Barrett–Joyner–Halenda (BJH) method. Pore size distribution (PSD) profiles were determined from the adsorption branch using the non-local density functional theory (NL DFT) method. The mean pore diameter (D_{av}) was calculated with the $D_{av} = 4V_{tot}/S_{BET}$ Gurvitch formula. The Specac mini pellet press (Specac Ltd., Orpington, UK) was used for pelletization of the composite powder. A combined thermogravimetric (TG) and differential scanning calorimetry (DSC) analysis was carried out in the flow of air (40 mL/min) with a STA 409 PC LUXX TG/DSC apparatus (Netzsch, Selb, Germany) in the temperature range of 30–1000 °C and at a heating rate of 10 °C/min.

3. Results and Discussion

3.1. Electron Microscopy Analysis

TEM and SEM micrographs of individual components used for the synthesis of composites are gathered in Figure 2. Figure 2a,b show TEM images of dried suspensions of CTA-Mt and Na-Mt, respectively. Both Mt dispersions are composed of very fine platelets. On average, the particles present in Na-Mt are thinner and smaller than those found in organoclay, pointing to the better dispersion of clay mineral suspension prepared by inverse microemulsion method. Figure 2c,d show a TEM and SEM image of TiO_2 nanoparticles prepared by inverse microemulsion. The material is composed of very fine, rounded grains of ca. 4–6 nm diameter (blown up images in Figure 2c).

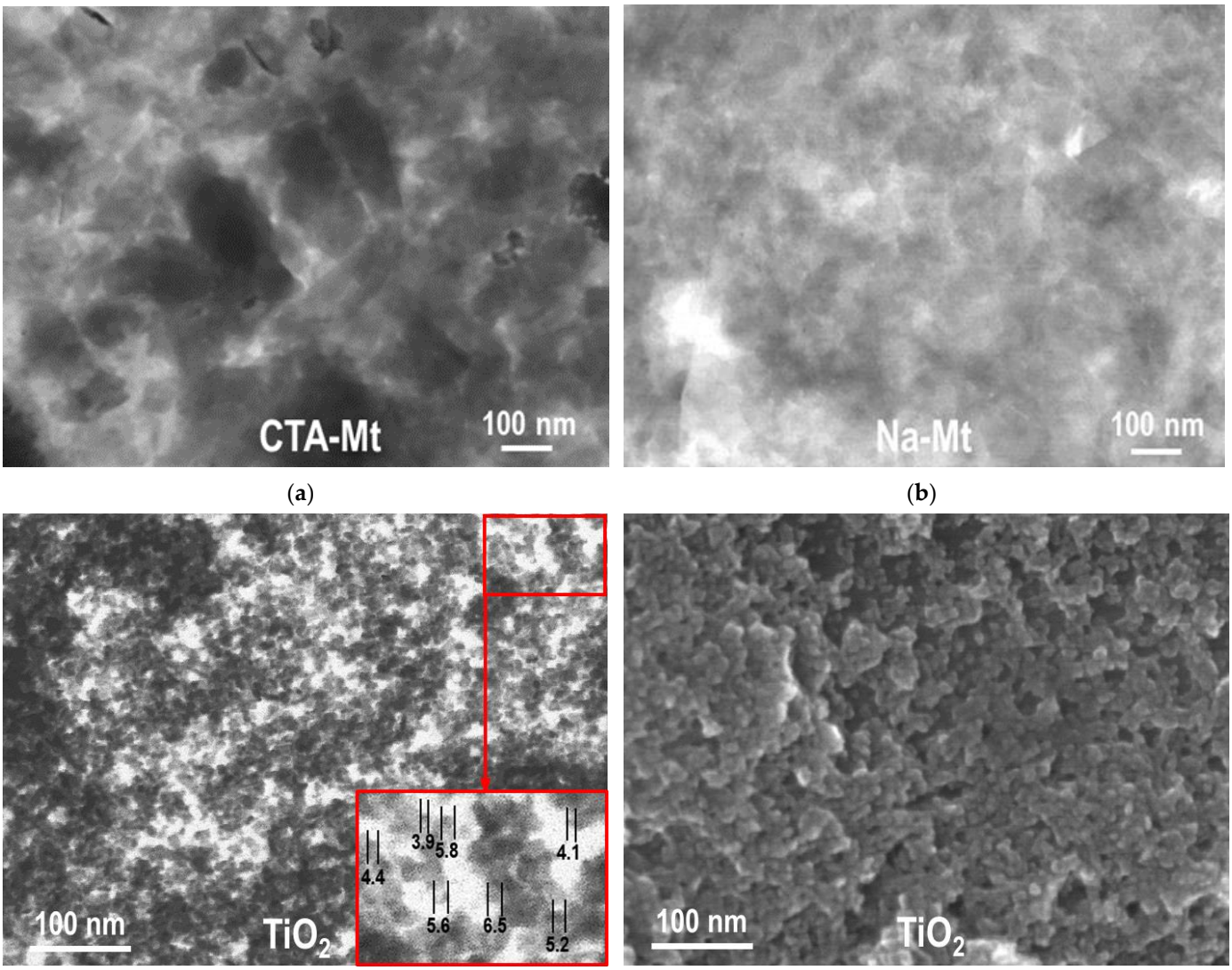

Figure 2. (**a**) TEM image of CTA-Mt; (**b**) TEM image of Na-Mt; (**c**) TEM image of titania obtained by inverse microemulsion method; (**d**) SEM image of titania obtained by inverse microemulsion method.

TEM analysis revealed differences between the TiO_2/CTA-Mt and TiO_2/Na-Mt series in the degree of intermixing of the two components. The effect observed for all members of the series is illustrated in Figure 3 with images of $1TiO_2$/CTA-Mt and $1TiO_2$/Na-Mt samples. In the micrographs, titania is visible as dark particles embedded in the clay mineral matrix. In $1TiO_2$/Na-Mt (Figure 3b), the titania nanoparticles are clearly better dispersed and quite homogeneously distributed. On the other hand, in $1TiO_2$/CTA-Mt (Figure 3a), agglomerates of TiO_2 species are more frequent, and the coverage of clay matrix by TiO_2 is less even. Results of the SEM/TEM study of individual components (Figure 2) suggest that the better intermixing of components in the TiO_2/Na-Mt series is likely to be due to the better dispersion/disintegration of the Na-Mt component. The reason for the observed effect may be differences in the preparation of suspensions of clay components. It is known that disintegration of Mt particles in the solvent is prompted by the swelling of clay mineral due to the penetration of solvent molecules into the interlayer. The resulting expansion of the interlayer spacing facilitates disassociation/exfoliation of clay particles. Swelling and exfoliation occurs both in the case of CTA-Mt dispersed in a suitable organic solvent and in the case of Na-Mt dispersed in water, but the phenomenon is much more efficient in the latter case [24]. Moreover, in contrast to the conventional dispersion of

CTA-Mt in 1-hexanol, in the Na-Mt microemulsion, the nanoparticles of exfoliated clay are held within the aqueous micellar cores and are, therefore, additionally stabilized against restacking and reaggregation.

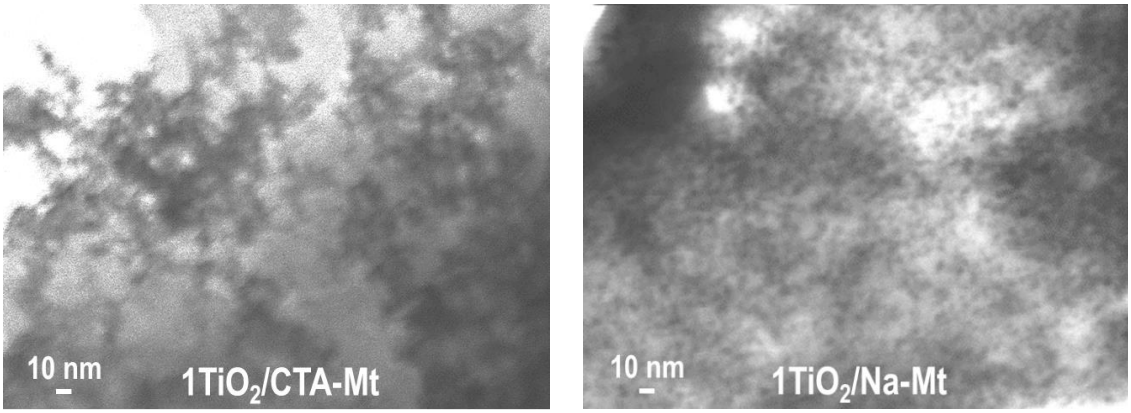

(**a**) (**b**)

Figure 3. TEM images of composites: (**a**) $1TiO_2$/CTA-Mt; (**b**) $1TiO_2$/Na-Mt.

The less homogeneous titania dispersion in the TiO_2/CTA-Mt series, compared to the TiO_2/CTA-Mt series, is also observed at the macroscale, as illustrated by SEM/EDX mapping of titanium and key clay structure-forming elements, i.e., Si, Al, and Mg, in $1TiO_2$/CTA-Mt and $1TiO_2$/Na-Mt composites. The results are shown in Figure 4. For a given composite, the mappings of Si, Al, and Mg mirror each other and reflect the texture/morphology of clay particles visible in SEM images. As for the distribution of Ti, it is evident that, in both samples, it is spread throughout the analyzed material, but only in $1TiO_2$/Na-Mt does the mapping of Ti replicate the sample texture/morphology in a similar way as the maps of clay-forming elements, pointing to a homogeneous intermixing of titania with the clay matrix. In $1TiO_2$/CTA-Mt, the match between the map of Ti and the maps of Si, Al, and Mg is much poorer, which indicates less even blending of titania nanoparticles with clay component.

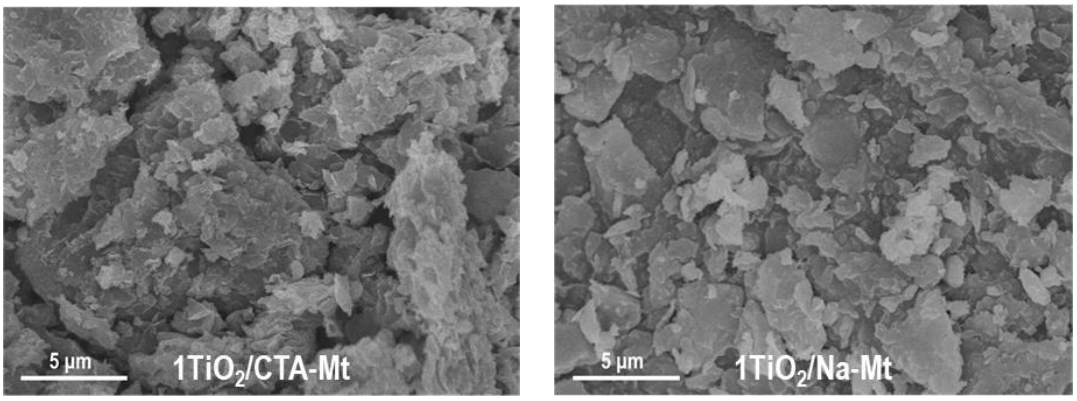

(**a**) (**b**)

Figure 4. *Cont.*

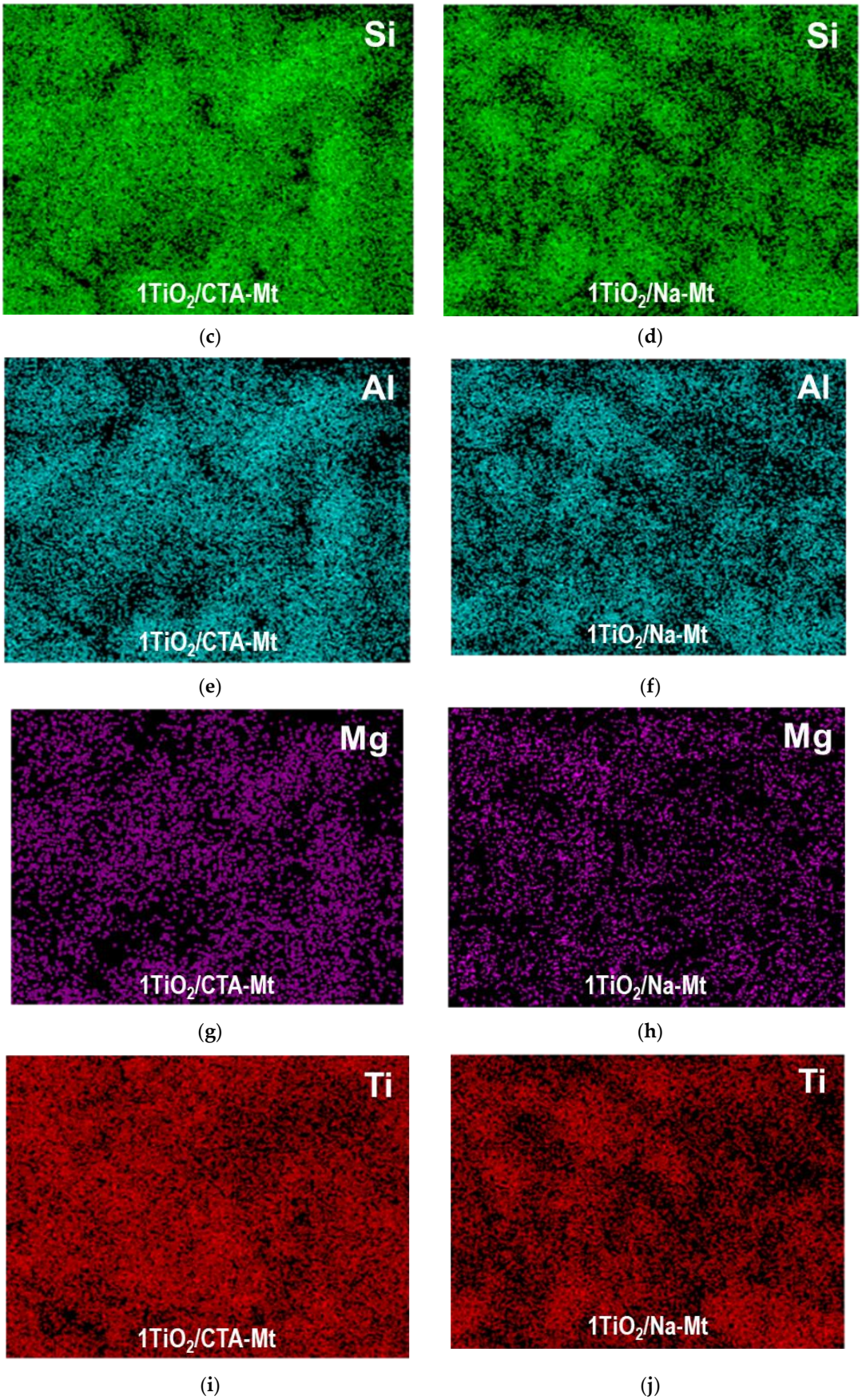

Figure 4. SEM/EDX compositional analysis of selected areas of $1TiO_2$/CTA-Mt and $1TiO_2$/Na-Mt

composites: (**a**) SEM image of 1TiO_2/CTA-Mt; (**b**) SEM image of 1TiO_2/Na-Mt; (**c**) EDX mapping image of Si in 1TiO_2/CTA-Mt; (**d**) EDX mapping image of Si in 1TiO_2/Na-Mt; (**e**) EDX mapping image of Al in 1TiO_2/CTA-Mt; (**f**) EDX mapping image of Al in 1TiO_2/Na-Mt; (**g**) EDX mapping image of Mg in 1TiO_2/CTA-Mt; (**h**) EDX mapping image of Mg in 1TiO_2/Na-Mt; (**i**) EDX mapping image of Ti in 1TiO_2/CTA-Mt; (**j**) EDX mapping image of Ti in 1TiO_2/Na-Mt.

3.2. X-ray Diffraction Analysis

XRD patterns of the investigated composite materials before and after calcination are shown in Figures 5 and 6, respectively. In all cases, reflections due to both composite components are visible. Thus, in the case of the non-calcined TiO_2/CTA-Mt series, montmorillonite reflections are observed, the intensity of which decreases with growing titania loading, as well as reflections assignable to poorly crystalline anatase modification, the intensity of which increases with Ti content. The result shows that hydrolysis of Ti precursor leads to the formation of some poorly crystalline titania already prior to calcination. The non-calcined 0.25TiO_2/CTA-Mt sample displays only the most intense (101) reflection of anatase at $2\Theta = 25.3^{\circ}$, but as the Ti loading increases, other anatase reflections become distinguishable (Figure 5a). In non-calcined 0.25TiO_2/CTA-Mt, the d_{001} basal spacing of Mt component is 1.73 nm, which is consistent with the bilayer conformation of aliphatic chains of organocation in the interlayer [25]. As TiO_2 loading grows, the d_{001} spacing of Mt becomes gradually lower to assume 1.39 nm in non-calcined 1.5TiO_2/CTA-Mt, which points to a monolayer arrangement of alkylammonium cations. The shift is attributed to the partial exchange of interlayer CTA^+ cations with hydronium ions stemming from the acidic aqueous cores of Ti inverse micelles. The lowering of CTA^+ content in the interlayer enables single-layer packing of organocations. Interestingly, the XRD patterns of non-calcined TiO_2/Na-Mt series show that instead of the basal spacing expected for sodium form of Mt (ca. 1.2 nm), the Mt component displays larger d_{001}, which is characteristic of an organoclay (Figure 5b). It is apparent that during preparation of Na-Mt dispersion by means of inverse micellar method, the CTABr surfactant acts as a source of organocations, leading to exchange of interlayer Na^+ with CTA^+. This conclusion is supported by the results of EDX experiments, which find no sodium in the TiO_2/Na-Mt composites (Table 1). The effect is advantageous, as in certain catalytic and photocatalytic applications, the presence of sodium impurity is detrimental [13,26]. As in the non-calcined TiO_2/CTA-Mt samples, a shift in the basal spacing from 1.75 to 1.42 nm is also observed in the TiO_2/Na-Mt composites, reflecting the gradual exchange of CTA^+ with hydronium ions.

Calcination of composites brings about two major changes in the XRD patterns of both series (Figure 6). First, the clay components display basal spacing d_{001} equal ca. 1 nm, characteristic of thermally collapsed Mt, and second, the reflections of anatase become more intense, indicating further crystallization of TiO_2 nanoparticles. The size of titania crystals, estimated by means of the Scherrer equation, is about 5–5.5 nm in both types of composites, which is comparable with the size of TiO_2 nanoparticles detected by electron microscopy.

Table 1. Chemical composition of investigated materials (based on EDX analysis) and textural parameters from N_2 adsorption/desorption isotherms at −196 °C.

Sample	TiO_2 (wt. %)	SiO_2 (wt. %)	Al_2O_3 (wt. %)	MgO (wt. %)	Fe_2O_3 (wt. %)	Na_2O (wt. %)	S_{BET} (m^2g^{-1})	V_{tot} (cm^3g^{-1})	V_{meso} (cm^3g^{-1})	D_{av} (nm)	D_{dom} (nm)
0.25TiO_2/CTA-Mt	16.4	56.3	21.6	3.8	1.9	-	174	0.233	0.174	5.3	3.8
0.5TiO_2/CTA-Mt	35.1	43.6	16.5	2.8	2.0	-	184	0.217	0.160	4.7	4.6
1TiO_2/CTA-Mt	45.2	36.5	14.4	2.2	1.7	-	208	0.247	0.189	4.8	4.9
1.5TiO_2/CTA-Mt	59.7	27.0	10.2	1.9	1.2	-	194	0.246	0.208	5.1	5.2
0.25TiO_2/Na-Mt	17.5	55.7	21.3	3.8	1.7	-	223	0.321	0.259	5.8	4.4
0.5TiO_2/Na-Mt	37.4	42.4	16.0	2.7	1.5	-	245	0.313	0.248	5.1	4.9
1TiO_2/Na-Mt	48.3	34.9	13.7	1.9	1.2	-	256	0.321	0.263	5.0	5.2
1.5TiO_2/Na-Mt	63.9	24.4	9.4	1.4	0.9	-	231	0.314	0.274	5.5	5.7
calcined Na-Mt	-	65.6	24.9	4.5	2.1	2.9	47	0.129	0.111	11.1	4.6
calcined CTA-Mt	-	66.5	25.8	4.9	2.8	-	92	0.168	0.136	7.3	4.0
calcined TiO_2	100.0	-	-	-	-	-	12	0.079	0.079	26.4	5.8

S_{BET}, BET-specific surface area; V_{tot}, total pore volume; V_{meso}, BJH volume of mesopore; D_{av}, average pore dimension; D_{dom}, dominant pore size.

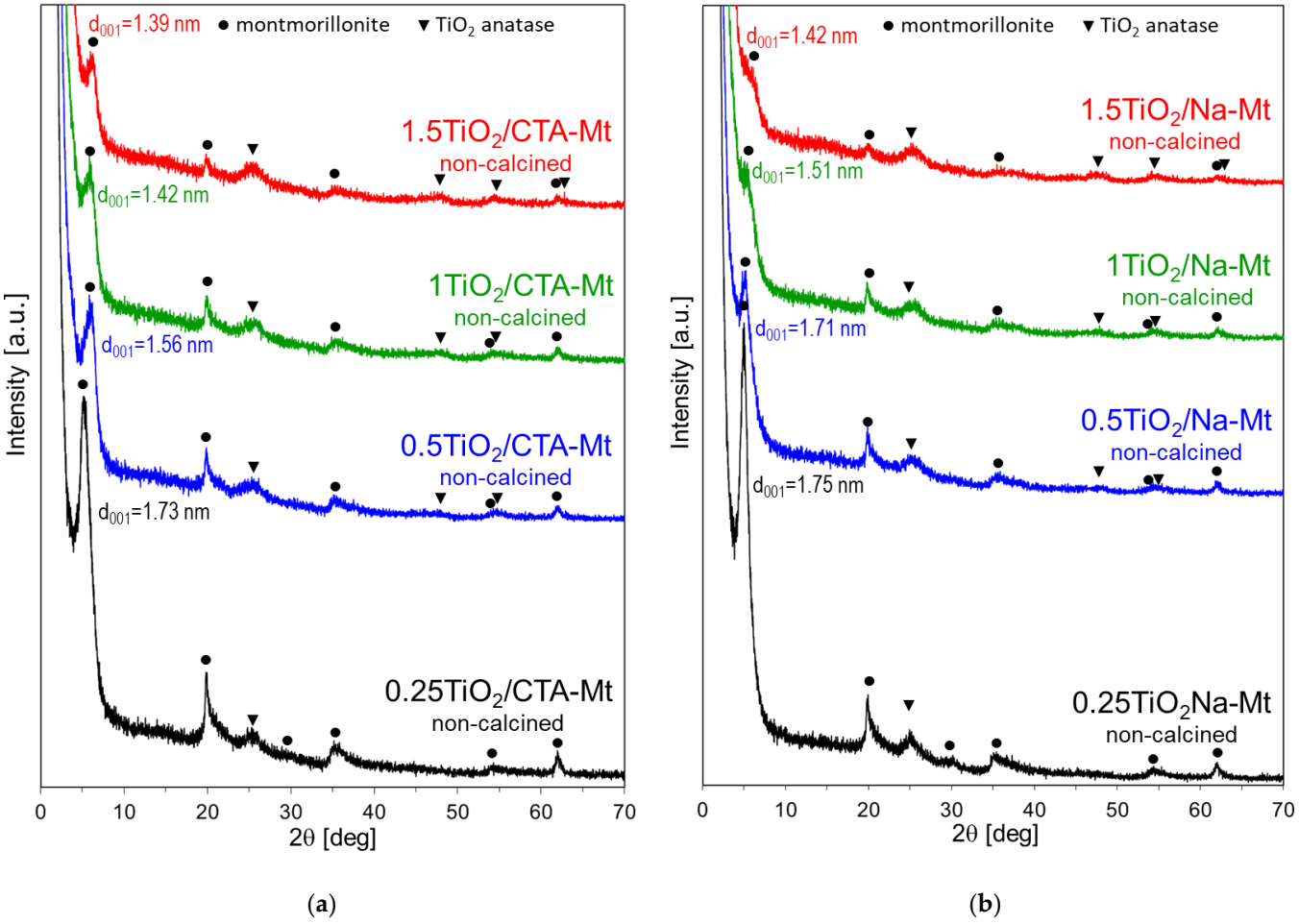

Figure 5. XRD patterns of non-calcined composites: (**a**) TiO_2/CTA-Mt and (**b**) TiO_2/Na-Mt; d_{001}—basal spacing of Mt component.

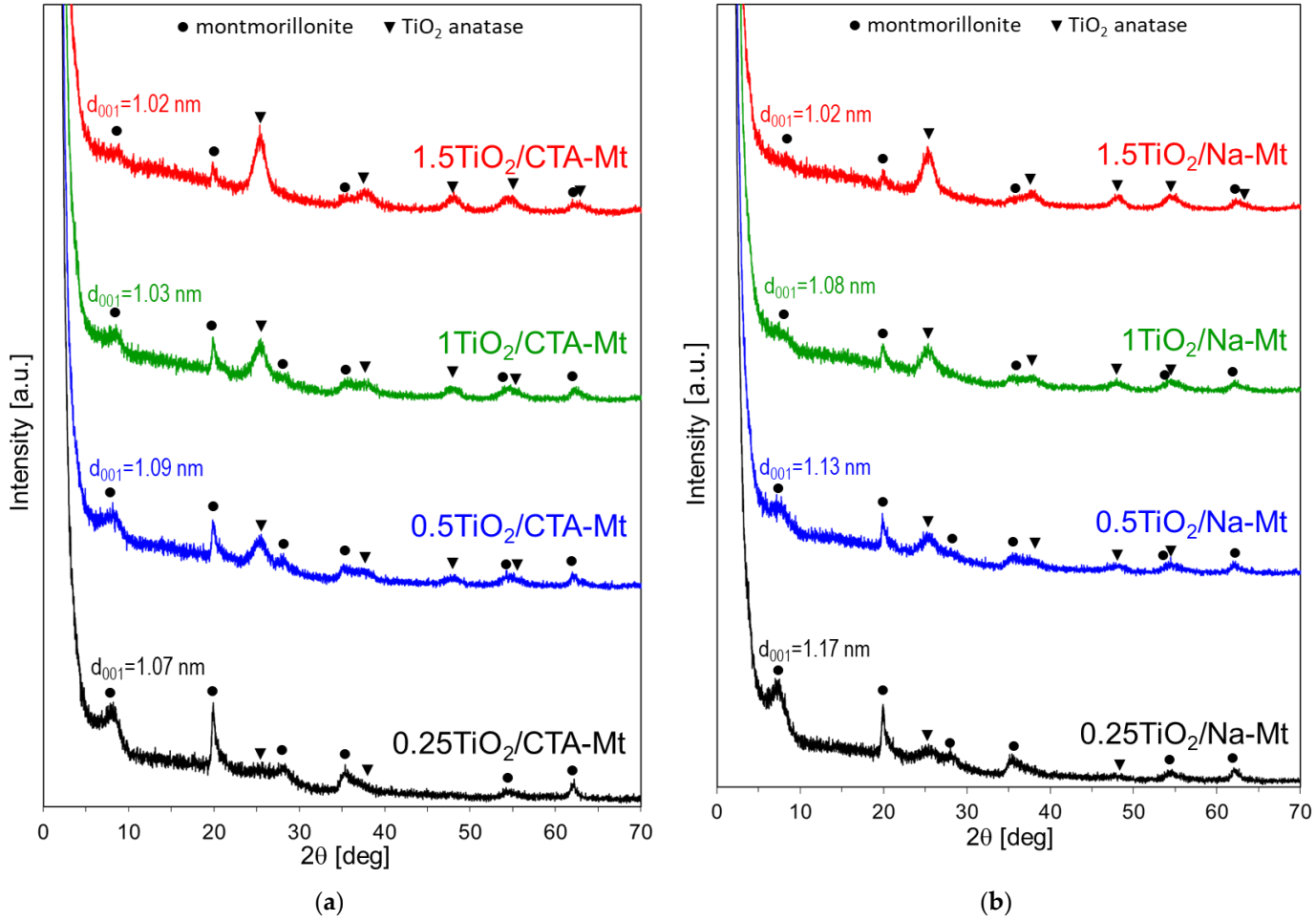

Figure 6. XRD patterns of calcined composites: (**a**) TiO_2/CTA-Mt and (**b**) TiO_2/Na-Mt; d_{001}—basal spacing of Mt component.

3.3. Thermal Analysis

Thermal evolution of non-calcined composites was studied by means of combined TG/DSC analysis, and the results are presented in Figure 7. Both series of composites show TG traces of similar shapes, and the total weight losses for the samples of analogous TiO_2 loadings are comparable (Figure 7a,b). This observation confirms that Na-Mt component underwent transformation to CTA-exchanged form during formation of microemulsion, so compositionally, both series of non-calcined composites are alike. Three stages of thermal decomposition can be distinguished in TG traces, as marked in Figure 7a. In the first, below 180 °C, mass loss increases with TiO_2 loading, in the second, up to ca. 700 °C, the opposite trend is observed, i.e., the lower the TiO_2 content, the higher the mass loss, and in the third, the mass of the samples stabilizes, with total mass loss growing with increasing content of Mt. The observed effects may be explained by considering concurrent thermal decomposition of composite components, i.e., the organoclay and the oxy-hydroxide Ti species. In the first stage of decomposition, below 180 °C, dehydration of both components occurs and is accompanied by the endothermic effect with maximum around 100 °C (Figure 7c,d). However, the organoclay component is relatively hydrophobic, and numerous studies have shown that only little water is desorbed in this temperature range [27–29]. Thus, in the composites, the initial mass loss is dominated by the dehydration of the hydrous titania precursor, and it therefore increases with the intended TiO_2 loading. The second stage of mass loss is dominated by the oxidative decomposition of the surfactant molecules adsorbed at the Mt surface and present as interlayer CTA^+ cations. The process

occurs in several overlapping steps accompanied by strong exothermic effects, with the last maximum in the 540–570 °C range (Figure 7c,d) due to the combustion of charcoal deposit [30]. The mass loss due to the dehydroxylation of Mt layers, known to occur below 700 °C, cannot be distinguished from the principal mass loss caused by combustion of the organic matter. Additionally, the accompanying endothermic effect is obscured by the strong exothermic maxima related to the oxidation of the organic matter. It is noteworthy that in both series, the exothermic maximum marking the final combustion of the organic deposit shifts from ca. 570 to ca. 540 °C upon growing TiO_2 content, pointing to the catalytic action of titania. In the third stage of thermal evolution, the mass of the samples remains constant, and the exothermic effect around 950 °C is due to the recrystallization of decomposed montmorillonite lattice; hence, its magnitude diminishes with the falling share of Mt component.

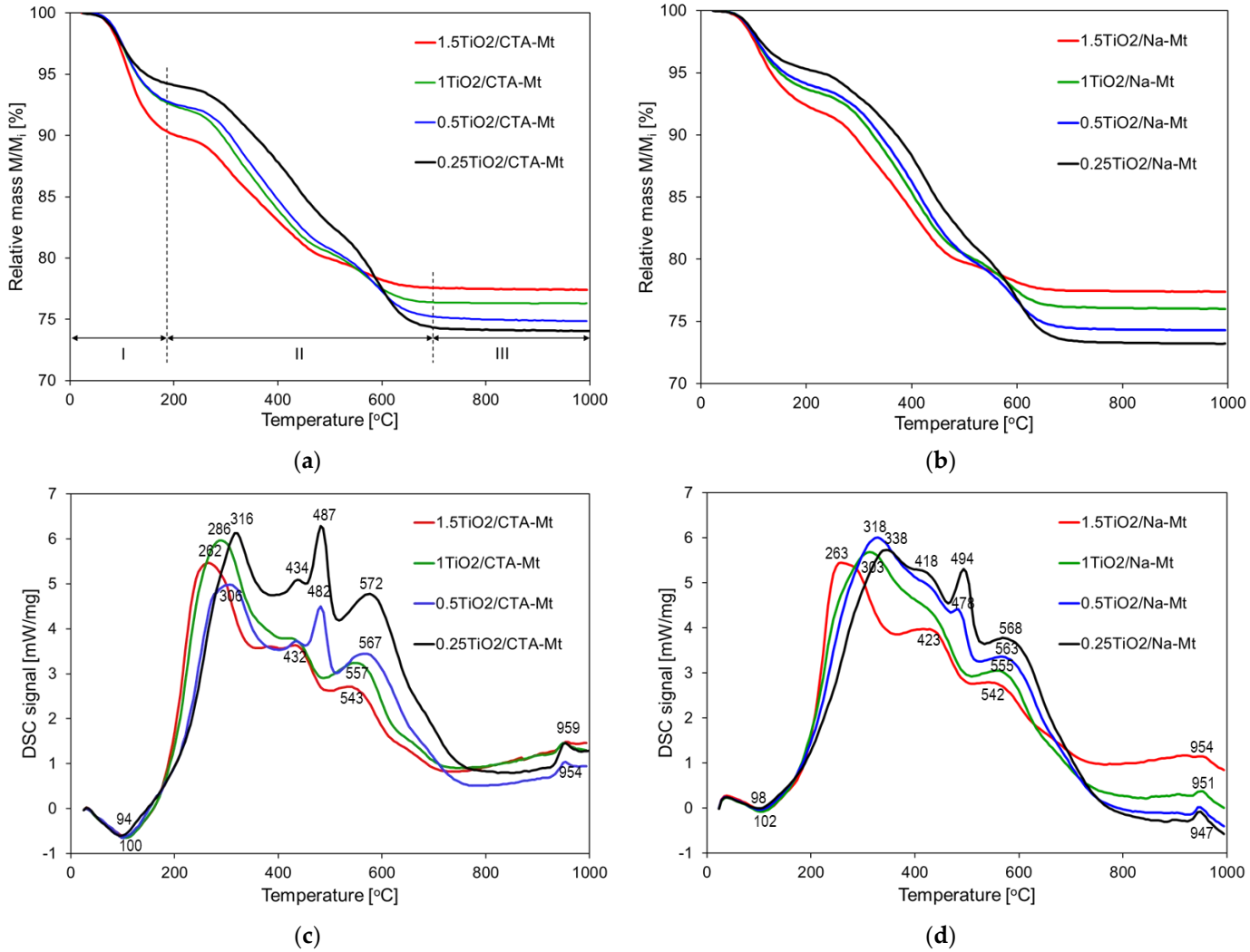

Figure 7. Thermal analysis of non-calcined composites: (**a**) TG of TiO_2/CTA-Mt samples; (**b**) TG of TiO_2/Na-Mt samples; (**c**) DSC of TiO_2/CTA-Mt samples; (**d**) DSC of TiO_2/Na-Mt.

3.4. Textural Properties

The nitrogen adsorption/desorption isotherms of TiO_2/CTA-Mt and TiO_2/Na-Mt series, together with the data obtained for individual components subjected to the same calcination procedure as the composites, are shown in Figure 8a,b, respectively. Textural parameters calculated from these graphs are presented in Table 1.

The shapes of adsorption isotherms of both series are very similar and may be classified as Type II, following the IUPAC classification [31]. All composites display pronounced hysteresis loops of H3 type, according to the same classification. The characteristic feature of H3 loop is that it closes at about p/p_0 = 0.42, which is typical of cavitation-induced pore emptying. Loops of this type are given by non-rigid aggregates of plate-like particles, which is consistent with the house of cards structure. The isotherms resemble those of individual clay components but are shifted upwards, pointing to the higher adsorption capacity of the composites. The isotherm of the calcined TiO_2 component lies much lower and displays almost no hysteresis, which indicates low porosity and suggests the occurrence of sintering during thermal treatment. Besides similarities, there are also distinct differences between the TiO_2/CTA-Mt and TiO_2/Na-Mt series. The adsorption capacity of the latter is clearly higher, and larger hysteresis loops point to larger mesoporous volume. Indeed, the calculated values of the total pore volumes and the mesopore volumes gathered in Table 1 show that TiO_2/Na-Mt samples are characterized by higher V_{tot} values than their TiO_2/CTA-Mt counterparts and that in each case the difference results from the increase of V_{meso}. It is noteworthy that the texture of the composites is clearly better developed than that of calcined parent clays. The pore size distribution curves presented in Figure 8c,d show that the dominant pore size, indicated by the PSD curve maximum, shifts slightly to higher values as TiO_2 loading increases. The dominant pore sizes of samples with the lowest TiO_2 content, namely 0.25TiO_2/CTA-Mt and 0.25TiO_2/Na-Mt, are about 3.8 and 4.5 nm and thus are meaningfully lower than the calculated average pore dimensions of 5.3 and 5.8 nm, respectively (Table 1). In all samples with higher TiO_2 content, the values of the dominant pore size and the average pore dimension are pretty close, pointing to the uniform character of pore network in composites richer in titania component. It should be noted that the dominant pore dimensions, around 5 nm, are close to the size of TiO_2 particles determined by TEM analysis (4–6 nm) and to the anatase crystallite dimension estimated from XRD (5–5.5 nm), which may be taken as an indication that the presence of uniform TiO_2 grains formed within inverse micelles is the main factor shaping the mesoporosity of composites.

Textural properties of TiO_2/clay composites are of particular importance for potential applications, as the accessibility of titania by the reactants depends on the well-developed pore network. Table 2 enables comparison of specific surface area and pore volume of selected examples of titania-clay composites obtained according to various synthetic procedures described in the literature, with the relevant properties of materials synthesized in this study. As mentioned in the Introduction, TiO_2/clay composites prepared by pillaring are the most commonly studied. Synthesis variations are numerous and involve, among others, change of calcination temperature, the use of different pillaring agents, the application of hydrothermal treatment, the use of organoclay host, etc. It is known that although composites obtained by pillaring display high specific surface area and pore volume, their largely microporous character may result in reactants experiencing diffusional limitations [1,11,12,32]. Microporosity can be largely reduced during synthesis of titania-clay heterostructures, whereby the layered clay host becomes exfoliated [33]. Composites prepared by impregnation ensure good accessibility of titania but typically possess much lower specific surface and pore volume [34]. With respect to the value of specific surface area and the total pore volume, the samples synthesized in this work compare favorably with most of the presented examples. Moreover, the TiO_2/CTA-Mt and TiO_2/Na-Mt series, although well-developed texturally, are non-microporous and show uniform mesoporous profiles, which is the feature important in design of potential photocatalysts or catalysts. The 1TiO_2/Na-Mt powder with the best-developed specific surface area and pore volume was tested for resistance of porous texture to mechanical stress by subjection to 1-ton pressure in a hydraulic press. The material proved quite robust, as its specific surface area remained almost unchanged (250 vs. 256 m^2g^{-1} before compression), while the total pore volume diminished by ca. 20% (0.261 vs. 0.321 cm^3g^{-1} before compression).

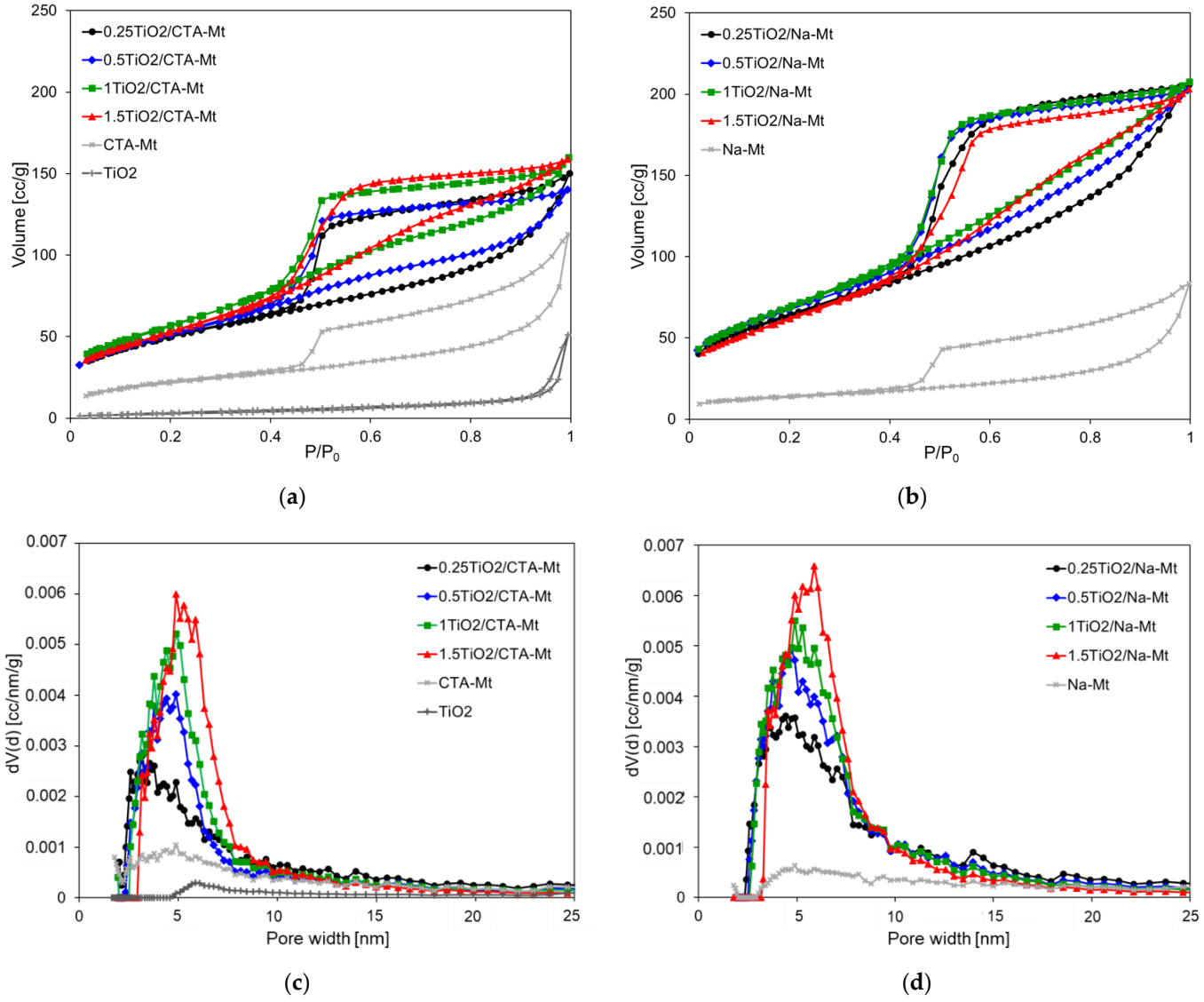

Figure 8. N_2 adsorption/desorption isotherms at –196 °C of: (**a**) TiO_2/CTA-Mt; (**b**) TiO_2/Na-Mt. Differential pore size distribution (dV(**d**)) of: (**c**) TiO_2/CTA-Mt; (**d**) TiO_2/Na-Mt.

It should be recalled that the interest in the development of titania-based nanocomposites is not limited to photocatalysis and catalysis but also stems from their wide application in photovoltaics, hydrogen storage, sensors, biomedicine, and electronics [1,8–12,40–46]. The synthetic procedure described in this work is aimed specifically at the formation of titanium-clay hybrid systems but can be readily adapted to the deposition of TiO_2 nanoparticles in a variety of matrices or can be used to prepare finely dispersed clay nanoparticles for potential use in other clay-based composites such as, e.g., clay-reinforced polymers. The proposed preparative approach can therefore inspire the design and fabrication of novel hybrid systems with potential well beyond the application areas of TiO_2/clay composites [47].

Table 2. Comparison of textural properties of TiO_2/Mt composites obtained by various methods reported in the literature with those of the materials synthesized in this study.

Method of TiO_2–Mt Composite Preparation	S_{BET} (m^2g^{-1})	V_{tot} (cm^3g^{-1})	Reference
Pillaring of Mt with $TiCl_4$ precursor, calcination 400 °C	379	0.392	[35]
Pillaring of Mt with $TiCl_4$ precursor, hydrothermal treatment 115 °C calcination 500 °C	135	0.303	[36]
Pillaring of Mt with $Ti(OC_3H_7)_4$ precursor, hydrothermal treatment 60 °C, calcination 500 °C	183	0.19	[37]
Pillaring of Mt with $Ti(OC_4H_9)_4$ precursor, calcination 450 °C	133	0.335	[38]
Pillaring of CTA-Mt with $Ti(OC_3H_7)_4$ precursor, calcination 500 °C	194	0.165	[39]
Porous clay heterostructure synthesis with $Ti(OC_3H_7)_4$ precursor and commercial organoclay Cloisite®30B, calcination 550 °C	143	0.210	[33]
Mt impregnated with $TiCl_4$ precursor, calcination at 350 °C	52	0.144	[34]
$TiCl_4$ precursor hydrolyzed within inverse micelles, mixed with exfoliated CTA-Mt, calcination 550 °C	208	0.247	this work
$TiCl_4$ precursor hydrolyzed within inverse micelles, mixed with Na-Mt dispersed in inverse microemulsion, calcination 550 °C	256	0.321	this work

S_{BET}, BET-specific surface area; V_{tot}, total pore volume.

4. Conclusions

The method of TiO_2/clay composite synthesis proposed in this work bases on the use of microemulsion technique for the synthesis of TiO_2 component and/or preparation of clay dispersion. The adopted procedure yielded uniform, rounded TiO_2 particles of 4–6 nm diameter. The new approach enabled dispersion of hydrophilic Na-Mt in an organic medium by formation of inverse microemulsion with clay particles present in aqueous micellar cores. The procedure resulted in the Na-Mt transformation to CTA-exchanged Mt. In consequence, both the composites derived from the parent CTA-Mt and the ones obtained from the Na-Mt component were compositionally similar. However, preparation of Na-Mt in microemulsion led to better disintegration of clay particles than the exfoliation treatment of CTA-Mt in an organic solvent. This resulted in the TiO_2/Na-Mt series showing superior intermixing of clay component with titania nanoparticles and ensured formation of composites with better-developed pore networks while retaining similar pore size distribution characteristics. The advantage of the adopted synthesis method is the formation of essentially mesoporous materials, with significant specific surface area and uniform mesoporosity determined by the size of titania nanoparticles. Given that the size of the inverse micelles can be modified by appropriate selection of the synthesis conditions, this method offers the possibility to control the dimensions of the nanoparticles formed in the micellar cores. This aspect of TiO_2/clay mineral synthesis as well as the photocatalytic properties of composites synthesized according to the procedure described in this paper are the matter of our current work.

Author Contributions: Conceptualization, E.M.S.; data curation, A.M., B.D.N., D.D. and A.W.; methodology, A.M. and E.M.S.; validation, A.M., B.D.N., D.D. and A.W.; investigation, A.M., B.D.N., D.D. and A.W.; writing—original draft preparation, E.M.S., writing—review and editing, E.M.S. and

A.W.; supervision, E.M.S.; project administration, E.M.S.; funding acquisition, E.M.S. All authors have read and agreed to the published version of the manuscript.

Funding: This research was funded by the Polish National Science Center (NCN), grant OPUS 2018/31/B/ST5/03292.

Institutional Review Board Statement: Not applicable.

Informed Consent Statement: Not applicable.

Data Availability Statement: The data presented in this study are available on request from the corresponding author.

Conflicts of Interest: The authors declare no conflict of interest. The funders had no role in the design of the study; in the collection, analyses, or interpretation of data; in the writing of the manuscript, or in the decision to publish the results.

References

1. Serwicka, E.M. Titania-clay mineral composites for environmental catalysis and photocatalysis. *Catalysts* **2021**, *11*, 1087. [CrossRef]
2. Fernández-García, M.; Rodriguez, J.A. Metal Oxide Nanoparticles. In *Encyclopedia of Inorganic Chemistry*; John Wiley & Sons, Ltd.: Hoboken, NJ, USA, 2009.
3. Myakonkaya, O.; Hu, Z.; Nazar, M.F.; Eastoe, J. Recycling Functional Colloids and Nanoparticles. *Chem. Eur. J.* **2010**, *16*, 11784–11790. [CrossRef] [PubMed]
4. Argyle, M.D.; Bartholomew, C.H. Heterogeneous Catalyst Deactivation and Regeneration: A Review. *Catalysts* **2015**, *5*, 145–269. [CrossRef]
5. Shan, A.Y.; Ghazi, T.I.M.; Rashid, S.A. Immobilisation of titanium dioxide onto supporting materials in heterogeneous photocatalysis: A review. *Appl. Catal. A Gen.* **2010**, *389*, 1–8. [CrossRef]
6. Serwicka, E.M.; Bahranowski, K. Environmental catalysis by tailored materials derived from layered minerals. *Catal. Today* **2004**, *90*, 85–92. [CrossRef]
7. Schoonheydt, R.A.; Johnston, C.T.; Bergaya, F. Clay minerals and their surfaces. In *Developments in Clay Science*; Schoonheydt, R., Johnston, C.T., Bergaya, F., Eds.; Elsevier: Amsterdam, The Netherlands, 2018; Volume 9, pp. 1–21.
8. Szczepanik, B. Photocatalytic degradation of organic contaminants over clay-TiO_2 nanocomposites: A review. *Appl. Clay Sci.* **2017**, *141*, 227–239. [CrossRef]
9. Mishra, A.; Mehta, A.; Basu, S. Clay supported TiO_2 nanoparticles for photocatalytic degradation of environmental pollutants: A Review. *J. Environ. Chem. Eng.* **2018**, *6*, 6088–6107. [CrossRef]
10. Deepracha, S.; Vibulyaseak, K.; Ogawa, M. Chapter 2.1: Complexation of TiO_2 with clays and clay minerals for hierarchically designed functional hybrids. In *Advanced Supramolecular Nanoarchitectonics*, 1st ed.; Ariga, K., Aono, M., Eds.; Elsevier: Amsterdam, The Netherlands, 2019; pp. 125–150.
11. Ruiz-Hitzky, E.; Aranda, P.; Akkari, M.; Khaorapapong, N.; Ogawa, M. Photoactive nanoarchitectures based on clays incorporating TiO_2 and ZnO nanoparticles. *Beilstein J. Nanotechnol.* **2019**, *10*, 1140–1156. [CrossRef]
12. Dlamini, M.C.; Maubane-Nkadimeng, M.S.; Moma, J.A. The use of TiO_2/clay heterostructures in the photocatalytic remediation of water containing organic pollutants: A review. *J. Environ. Chem. Eng.* **2021**, *9*, 106546. [CrossRef]
13. Napruszewska, B.D.; Michalik-Zym, A.; Rogowska, M.; Bielańska, E.; Rojek, W.; Gaweł, A.; Wójcik-Bania, M.; Bahranowski, K.; Serwicka, E.M. Novel montmorillonite/TiO_2/MnAl-mixed oxide composites prepared from inverse microemulsions as combustion catalysts. *Materials* **2017**, *10*, 1326. [CrossRef]
14. Napruszewska, B.D.; Michalik-Zym, A.; Dula, R.; Bielańska, E.; Rojek, W.; Machej, T.; Socha, R.P.; Lityńska-Dobrzyńska, L.; Bahranowski, K.; Serwicka, E.M. Composites derived from exfoliated Laponite and Mn-Al hydrotalcite prepared in inverse microemulsion: A new strategy for design of robust VOCs combustion catalysts. *Appl. Catal. B Environ.* **2017**, *211*, 46–56. [CrossRef]
15. Bahranowski, K.; Gaweł, A.; Klimek, A.; Michalik-Zym, A.; Napruszewska, B.D.; Nattich-Rak, M.; Rogowska, M.; Serwicka, E.M. Influence of purification method of Na-montmorillonite on textural properties of clay mineral composites with TiO_2 nanoparticles. *Appl. Clay Sci.* **2017**, *140*, 75–80. [CrossRef]
16. Ganguli, A.K.; Ganguly, A.; Vaidya, S. Microemulsion-based synthesis of nanocrystalline materials. *Chem. Soc. Rev.* **2010**, *39*, 474–485. [CrossRef]
17. Eastoe, J.; Hollamby, M.J.; Hudson, L. Recent advances in nanoparticle synthesis with reversed micelles. *Adv. Colloid Interface Sci.* **2006**, *128–130*, 5–15. [CrossRef]
18. Asgari, S.; Saberi, A.H.; McClements, D.J.; Lin, M. Microemulsions as Nanoreactors for Synthesis of Biopolymer Nanoparticles. *Trends Food Sci. Technol.* **2019**, *86*, 118–130. [CrossRef]
19. Kubacka, A.; Caudillo-Flores, U.; Barba-Nieto, I.; Muñoz-Batista, M.J.; Fernández-García, M. Microemulsion: A versatile synthesis tool for Photocatalysis. *Curr. Opin. Colloid Interface Sci.* **2020**, *49*, 42–59. [CrossRef]
20. Šucha, V.; Kraus, I. Natural microporous materials of central Slovakia. In *Natural Microporous Materials in Environmental Technology*; Misaelides, P., Macasek, F., Pinnavaia, T.J., Colella, C., Eds.; Kluwer Academic Press: Dordrecht, The Netherlands, 1999; pp. 101–107.

21. Ahmad, S.I.; Friberg, S. Catalysis in micellar and liquid-crystalline phases. I. System water-hexadecyltrimethylammonium bromide-hexanol. *J. Am. Chem. Soc.* **1972**, *94*, 5196–5199. [CrossRef]
22. Tai, C.Y.; Hsiao, B.Y.; Chiu, H.Y. Preparation of spherical hydrous-zirconia nanoparticles by low temperature hydrolysis in a reverse microemulsion. *Colloids Surf. A Physicochem. Eng. Asp.* **2004**, *237*, 105–111. [CrossRef]
23. Sterte, J. Synthesis and properties of titanium oxide cross-linked montmorillonite. *Clays Clay Miner.* **1986**, *34*, 658–664. [CrossRef]
24. Zhu, T.T.; Zhou, C.H.; Kabwe, F.B.; Wu, Q.Q.; Li, C.S.; Zhang, J.R. Exfoliation of montmorillonite and related properties of clay/polymer nanocomposites. *Appl. Clay Sci.* **2019**, *169*, 48–66. [CrossRef]
25. Lagaly, G.; Ogawa, M.; Dékány, I. Clay mineral–organic interactions; chapter 10.3. In *Handbook of Clay Science*; Bergaya, F., Lagaly, G., Eds.; Elsevier: Amsterdam, The Netherlands, 2013; Volume 5, pp. 435–505.
26. Xie, H.; Li, N.; Liu, B.S.; Yang, J.J.; Zhao, X.J. Role of sodium ion on TiO_2 photocatalyst: Influencing crystallographic properties or serving as the recombination center of charge carriers? *J. Phys. Chem. C* **2016**, *120*, 10390–10399. [CrossRef]
27. Hedley, C.; Yuan, G.; Theng, B. Thermal analysis of montmorillonites modified with quaternary phosphonium and ammonium surfactants. *Appl. Clay Sci.* **2007**, *35*, 180–188. [CrossRef]
28. Pálková, H.; Madejová, J.; Zimowska, M.; Bielańska, E.; Olejniczak, Z.; Lityńska-Dobrzyńska, L.; Serwicka, E.M. Laponite-derived porous clay heterostructures: I. Synthesis and physicochemical characterization. *Micropor. Mesopor. Mater.* **2010**, *127*, 228–236. [CrossRef]
29. Andrunik, M.; Bajda, T. Modification of Bentonite with Cationic and Nonionic Surfactants: Structural and Textural Features. *Materials* **2019**, *12*, 3772. [CrossRef] [PubMed]
30. Yariv, S. The role of charcoal on DTA curves of organo-clay complexes: An overview. *Appl. Clay Sci.* **2004**, *24*, 225–236. [CrossRef]
31. Thommes, M.; Kaneko, K.; Neimark, A.V.; Olivier, J.P.; Rodriguez-Reinoso, F.; Rouquerol, J.; Sing, K.S.W. Physisorption of gases, with special reference to the evaluation of surface area and pore size distribution (IUPAC Technical Report). *Pure Appl. Chem.* **2015**, *87*, 1052–1069. [CrossRef]
32. Gil, A.; Vicente, M.A. Progress and perspectives on pillared clays applied in energetic and environmental remediation processes. *Curr. Opin. Green Sustain. Chem.* **2020**, *21*, 56–63. [CrossRef]
33. Belver, C.; Bedia, J.; Rodriguez, J.J. Titania–clay heterostructures with solar photocatalytic applications. *Appl. Catal. B Environ.* **2015**, *176–177*, 278–287. [CrossRef]
34. Djellabi, R.; Ghorab, M.F.; Cerrato, G.; Morandi, S.; Gatto, S.; Oldani, V.; Di Michele, A.; Bianchi, C.L. Photoactive TiO2–montmorillonite composite for degradation of organic dyes in water. *J. Photochem. Photobiol. A Chem.* **2014**, *295*, 57–63. [CrossRef]
35. Michalik-Zym, A.; Dula, R.; Duraczńyska, D.; Kryściak-Czerwenka, J.; Machej, T.; Socha, R.P.; Włodarczyk, W.; Gaweł, A.; Matusik, J.; Bahranowski, K.; et al. Active, selective and robust Pd and/or Cr catalysts supported on Ti-, Zr- or [Ti,Zr]-pillared montmorillonites for destruction of chlorinated volatile organic compounds. *Appl. Catal. B-Environ.* **2015**, *174–175*, 293–307. [CrossRef]
36. Butman, M.F.; Ovchinnikov, N.L.; Karasev, N.S.; Kochkina, N.E.; Agafonov, A.V.; Vinogradov, A.V. Photocatalytic and adsorption properties of TiO_2-pillared montmorillonite obtained by hydrothermally activated intercalation of titanium polyhydroxo complexes. *Beilstein J. Nanotechnol.* **2018**, *9*, 364–378. [CrossRef]
37. Belessi, V.; Lambropoulou, D.; Konstantinou, I.; Katsoulidis, A.; Pomonis, P.; Petridis, D.; Albanis, T. Structure and photocatalytic performance of TiO_2/clay nanocomposites for the degradation of dimethachlor. *Appl. Catal. B Environ.* **2007**, *73*, 292–299. [CrossRef]
38. Chen, J.; Liu, X.; Li, G.; Nie, X.; An, T.; Zhang, S.; Zhao, H. Synthesis and characterization of novel SiO2 and TiO2 co-pillared montmorillonite composite for adsorption and photocatalytic degradation of hydrophobic organic pollutants in water. *Catal. Today* **2011**, *164*, 364–369. [CrossRef]
39. Chen, D.; Du, G.; Zhu, Q.; Zhou, F. Synthesis and characterization of TiO_2 pillared montmorillonites: Application for methylene blue degradation. *J. Colloid Interface Sci.* **2013**, *409*, 151–157. [CrossRef]
40. Sang, L.; Zhao, Y.; Burda, C. TiO_2 Nanoparticles as Functional Building Blocks. *Chem. Rev.* **2014**, *114*, 9283–9318. [CrossRef]
41. Noman, M.T.; Ashraf, M.A.; Ali, A. Synthesis and applications of nano-TiO_2: A review. *Environ. Sci. Pollut. Res.* **2019**, *26*, 3262–3291. [CrossRef]
42. Yang, H.; Yang, B.; Chen, W.; Yang, J. Preparation and Photocatalytic Activities of TiO_2-Based Composite Catalysts. *Catalysts* **2022**, *12*, 1263. [CrossRef]
43. Tian, X.; Cui, X.; Lai, T.; Ren, J.; Yang, Z.; Xiao, M.; Wang, B.; Xiao, X.; Wang, Y. Gas sensors based on TiO_2 nanostructured materials for the detection of hazardous gases: A review. *Nano Mater. Sci.* **2021**, *3*, 390–403. [CrossRef]
44. Padmanabhan, N.T.; Thomas, N.; Louis, J.; Mathew, D.T.; Ganguly, P.; John, H.; Pillai, S.C. Graphene coupled TiO_2 photocatalysts for environmental applications: A review. *Chemosphere* **2021**, *271*, 129506. [CrossRef]
45. Paul, S.; Rahman, M.A.; Sharif, S.B.; Kim, J.; Siddiqui, S.; Hossain, M.A.M. TiO_2 as an anode of high-performance lithium-ion batteries: A comprehensive review towards practical application. *Nanomaterials* **2022**, *12*, 2034. [CrossRef]
46. Javed, R.; Ain, N.U.; Gul, A.; Ahmad, M.A.; Guo, W.; Ao, Q.; Tian, S. Diverse biotechnological applications of multifunctional titanium dioxide nanoparticles: An up-to-date review. *IET Nanobiotechnol.* **2022**, *16*, 171–189. [CrossRef] [PubMed]
47. Hassan, T.; Salam, A.; Khan, A.; Khan, S.U.; Khanzada, H.; Wasim, M.; Khan, M.Q.; Kim, I.S. Functional nanocomposites and their potential applications: A review. *J. Polym. Res.* **2021**, *28*, 36. [CrossRef]